J Mater Sci (2007) 42:1890–1900
DOI 10.1007/s10853-006-1322-y



# Non-stoichiometry and electronic properties of interfaces

**A. Klein · F. Säuberlich · B. Späth · T. Schulmeyer · D. Kraft**

Received: 30 November 2005 / Accepted: 1 March 2006 / Published online: 9 January 2007


**Abstract** The paper gives an overview on the influence of point defects on electronic properties of interfaces including band alignment (barrier heights) and transport properties. As examples interfaces between metals and the II–VI semiconductors CdTe and ZnTe are presented. In addition untypical phenomena at semiconductor heterocontact formation at $In_2S_3$/ZnO and $CuInSe_2$/CdS interfaces is described. It is suggested that the barrier heights as well as the transport properties at both interfaces are strongly affected by defects, which are either present because of non-stoichiometry of the materials or introduced by contact formation due to chemical interactions.

## Defects and interfaces

Electronic properties of interfaces determine the function of electronic devices [1–4]. Important features of interfaces are the barrier heights, the current transport across the interface, charge injection and minority carrier recombination. Current transport across an interface is mainly affected by the barrier heights but can also be strongly modified in the presence of defect states in the band gap not only by modifying the potential distribution, but also by adding additional transport paths involving recombination or tunnelling utilizing defect states [4, 5].

Electronic devices are, in most cases, made with materials having a fundamental band gap as semiconductors or insulators. The interface properties of insulating materials as dielectrics, ferroelectrics and others should therefore, in principle, be described by the same fundamental mechanisms as developed for semiconductors. An energy band diagram for a n-type semiconductor/metal interface is shown in Fig. 1. The barrier height $\Phi_B$ for electrons (holes) at a semiconductor/metal interface, which is given by the distance between the Fermi energy at the interface and the conduction (valence) band edge, largely determines the electronic properties of the contact.

Extensive research has been devoted in the past to understand the mechanisms governing barrier formation at semiconductor interfaces in order to enable prediction and possible modification of barrier heights [1, 6–11]. Considerable complication in this is induced by *Fermi level pinning*, which results in barrier heights being almost independent of the contact metal. Fermi level pinning is mostly pronounced for semiconductors with covalent bonding such as Si, Ge and GaAs and less strong for polar bonded materials as oxides [12]. It is phenomenologically accounted for by the presence of *interface states* in the semiconductor [3, 13] as indicated in Fig. 1. The interface states give rise to an additional charge located within a few Angstroms at the interface. The charge associated with these interface states can be either positive or negative, depending on the Fermi level position relative to the *charge neutrality level* $E_{CNL}$, which is associated with the interface states. There is no charge in the interface states if $E_F = E_{CNL}$. A negative (positive) charge will

A. Klein (✉) · F. Säuberlich · B. Späth · T. Schulmeyer · D. Kraft
Institut für Materialwissenschaft, Fachgebiet Oberflächenforschung, Technische Universität Darmstadt, Petersenstrasse 23, 64287 Darmstadt, Germany
e-mail: aklein@surface.tu-darmstadt.de

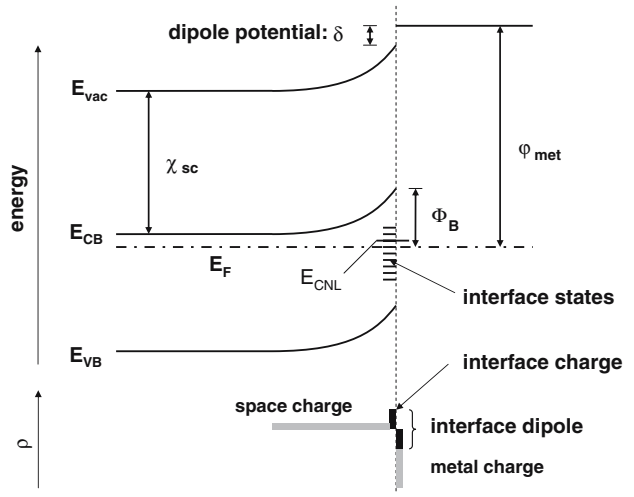


**Fig. 1** Potential and charge distribution at n-type semiconductor/metal interface. The barrier height $\Phi_B$ is given by the distance between the Fermi energy and the conduction band minimum. Charged interface states in the semiconductor induce an interface dipole, which leads to a dipole potential $\delta$. The sign of the charge of the interface states is defined by the position of the charge neutrality level $E_{CNL}$ with respect to the Fermi energy

occur if $E_F > (<) E_{CNL}$. The position of $E_{CNL}$ with respect to the band edges depends on the details of the distribution of interface states. For a high concentration of interface states the position of the charge neutrality level determines the Fermi level position at the interface and hence the barrier heights.

Charge neutrality levels have been calculated on the basis of fundamental bulk properties of the semiconductors [1, 14, 15], which rely on the basic picture of *metal-induced gap states* (MIGS) first introduced by Heine [16] and clearly evident from electronic structure calculations [17]. It needs to be mentioned that this generalized pictures does not account for some observed variations in barrier heights for a single material combination, which are related to the details of the atomic structure at the interface [9]. Nevertheless, the *induced gap states* concept gives a straightforward explanation for the occurrence of the interface states and Fermi level pinning even for interfaces, which are atomically abrupt and free of crystallographic point defects. In a chemical bonding picture, the MIGS are provided by the polarization of the lattice due to the distortion of the chemical bonds at the interface [18]. Consequently, the barrier heights can be regarded as being determined by the chemical bonds at the interface.

Barrier formation for the most important elemental and III–V semiconductors are well understood and generally discussed in terms of such abrupt junctions [1, 6–8]. For these materials, deviation from stoichiometry is not a big issue. This is due to the large energies required to create intrinsic crystallographic point defects as vacancies or interstitials. Therefore, the concentration of point defects should be negligible. However, Fermi level pinning at interfaces of GaAs has also been attributed to formation of anti-site defects during metal deposition [19, 20]. These are assumed to be created in consequence of the release of the condensation energy of the metal atoms. Alternatively, Walukiewicz suggested in an amphoteric defect model [21, 22] that point defects are created as a result of the movement of the Fermi level at the interface. This phenomenon is related to the self-compensation mechanism in semiconductors which leads to a limitation of achievable doping levels [23] and whose origin lies in the dependence of defect formation energies on the Fermi level position [24]. However, in most cases the role of point defects at interfaces of semiconductors is neglected.

Interfaces of polar bonded materials as chalcogenides, oxides and halides are expected to be considerably more influenced by point defects. One reason is given by the lower defect formation enthalpies of these materials. This can be rationalized from the fact that a vacancy or an interstitial in a III–V compound results in a mismatch of 3 electrons per defect site, compared to 2 electrons in chalcogenides and oxides and only 1 electron in halides. Consequently, vacancies and interstitials or their combinations (Frenkel and Schottky defects) are much more abundant in the latter materials. Lower defect formation enthalpies are also highlighted by the fact that non-stoichiometric materials typically exhibit polar bonding [25–27].

In most cases, polar bonded materials have larger band gaps than corresponding covalent materials. For example, the band gaps of Ge, GaAs and ZnSe are 0.7, 1.4 and 2.7 eV, respectively. Because of the larger band gaps of polar bonded materials, defect formation by self-compensation is also more important, since the larger the band gap, the larger the possible movement of the Fermi level at the interface.

The interface formation between covalent (stoichiometric) and polar (non-stoichiometric) materials is therefore suggested to be different because of different densities of *induced gap states* ($D_{IGS}$) and of crystallographic point defects states ($D_{cr}$). For covalent semiconductors $D_{IGS}$ is typically of the order of $10^{14}$ cm$^{-2}$ [1, 13, 28], roughly corresponding to 10% of a monolayer. Materials with larger band gaps show a lower density on induced gap states [17], which is in accordance with the observation of reduced Fermi level pinning at interfaces of such materials [12]. Interfaces of covalent materials therefore have a low

density of crystallographic point defects and a high density of induced gap states and will thus be dominated by induced gap states. In contrast, polar materials have a lower density of induced gap states and a higher density of crystallographic point defects and should therefore show a different behaviour. In both situations, barrier heights are determined by defect states at the interface as shown in Fig. 1. The different behaviour can be summarized as follows:

(1) If the influence of crystallographic point defects on barrier formation can be neglected, which is most likely the case for covalent materials, a certain material combination results in a unique barrier height. This is in general agreement with experiment [1, 6–11].
(2) For polar bonded materials the barrier heights should depend on the density of crystallographic point defects near the interface. This could be influenced by a different chemical reactivity at the interface or also by treatments in selective partial pressures. There are experimental observations at oxide/metal interfaces indicating that barrier heights change with processing conditions [29–32]. The band alignment at interfaces between GaAs or AlAs with ZnSe is also reported to strongly depend on the Se partial pressure [33]. However, the latter observation has been explained by different atomic structures at the interface and not by a different concentration of point defects.

Although the latter behaviour suggests that for polar materials the barrier heights can be modified by influencing the density of point defects at the interface, there is not a complete degree of freedom in moving $E_F$, since self-compensation will also limit the movement of the Fermi level.

## Experimental approaches

### Photoemission experiments

Photoemission experiments (XPS, UPS) have contributed significantly to the understanding of barrier formation since they allow for a simultaneous investigation of chemical and electronic properties of interfaces. A typical photoemission interface experiment starts with preparation of a substrate surface and then repeated deposition steps of a contact material [34, 35]. Because of the high surface sensitivity of photoemission (typically 1–3 nm) and the immediate changes of the surface properties with deposition, film thickness is typically controlled down to submonolayer coverage. After each deposition step, both chemical and electronic changes are monitored. To avoid possible disturbance of the results by unwanted adsorbates, such experiments are conducted using integrated surface analysis and preparation systems, which allow for a vacuum transfer between deposition and analysis.

While the chemical sensitivity of XPS is a well-known property of this technique [36], determination of barrier heights relies on its possibility to determine electronic surface potentials. Typically the Fermi level, which is derived from the measurement of a metallic sample, serves as the reference for the binding energies. Therefore, the distance between the valence band maximum and the Fermi energy at the surface can be directly read from valence band spectra (see Fig. 2). Since for typical doping levels of semiconductors the width of depletion layers (~100 nm [3]) is large compared to the information depth of XPS and UPS (1–3 nm [36]), a change of surface potential by band bending gives rise to a parallel shift of all binding energies (see Fig. 2). Hence, it is possible to monitor the change of the Fermi level during interface formation.

Photoemission experiments typically reveal no direct information about defects at interfaces. Indirect evidence for defects is given by the occurrence of new chemical species due to interface reactions and by shifts of the Fermi level. For selected cases, temperature dependent photovoltage measurements can indicate that defects, which cannot be determined directly,

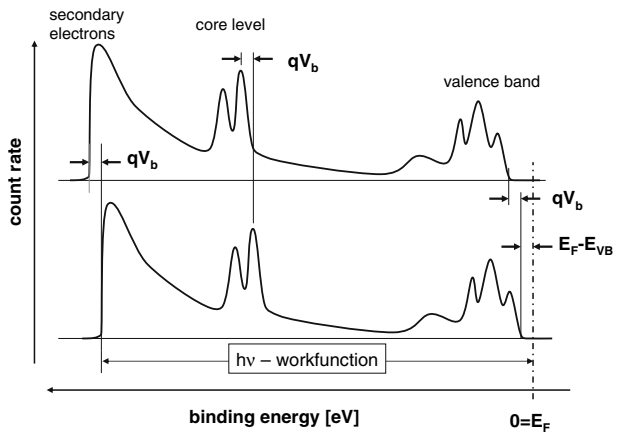


**Fig. 2** Typical photoemission spectra showing the determination of surface potentials. The binding energy reference in photoemission is typically the Fermi energy, whose position can be determined using a metallic sample. For semiconducting samples, changes of the band edges at the surface with respect to the Fermi energy, e.g. by an induced band bending $qV_b$, give rise to a rigid shift of all emissions

are introduced by interface formation [37]. This observation is possible since photovoltages also lead to binding energy shifts. The magnitude of the photovoltage and particularly its temperature dependence then depends on the charge transport across the interface, which is strongly affected by defects (see following section).

### Electrical transport properties

Electrical measurements are amongst the most sensitive experimental techniques. A modification of a barrier height by only 100 meV, hardly detectable using photoemission, leads to a change in current density by $e^{0.1\ eV/kT}$, which amounts to a factor of 50 at room temperature. This is due to the thermal excitation of most transport properties. The transport processes, which contribute to the current density at a semiconductor/metal interface, are schematically shown in Fig. 3 [38]. In many cases, the dominant contribution comes from thermionic emission of carriers over the barrier (process (i)). For this case the current density is described by the well-known Eq. 1

$$j = A^* T^2 e^{-\Phi_B/kT}(e^{qV/kT} - 1) \quad (1)$$

where $A^* = m^* \times 1.2 \times 10^5\ \mathrm{mA/cm^2K^2}$ is the effective Richardson constant with the (relative) effective mass $m^*$ of the charge carriers.

Process (ii) in Fig. 3 represents a tunnel-assisted thermionic emission, also known as thermionic field emission and process (iv) minority carrier injection. While the latter can in most cases be neglected, thermionic field emission dominates for high doping levels, where the space charge region becomes narrow. The third process (iii) represents recombination in the space charge region. Analytical expressions for this transport process can be given under simplifying assumptions [4, 38]

$$j = \frac{Wn_i}{2\tau}(e^{qV/nkT} - 1) \quad (2)$$

where $W$ is the width of the space charge region, $n_i$ the intrinsic carrier concentration and $\tau$ the minority carrier lifetime in the space charge region. The value $n$ in the denominator is a *diode ideality factor*, which should vary between 1 and 2 for this process [4, 38]. For large band gap materials $n_i$ becomes quite small and the process should not contribute significantly to the current transport. In such cases, theoretical models developed to describe transport and tunnelling processes in disordered solids might be more appropriate [5]. This might include mostly hopping transport based on tunnelling between defect states.

The major limitation of electrical measurement techniques, as current–voltage or capacitance–voltage measurements, is that they are affected by a number of parameters and that different transport mechanisms are described by similar expressions. In many cases, it is only possible to distinguish between different influences and identify the transport mechanism unambiguously if some parameters are known from other experiments. In this respect, the situation for non-stoichiometric materials is most complex as defects can not be avoided, their concentration depends on processing and they affect both the barrier heights and the transport mechanism.

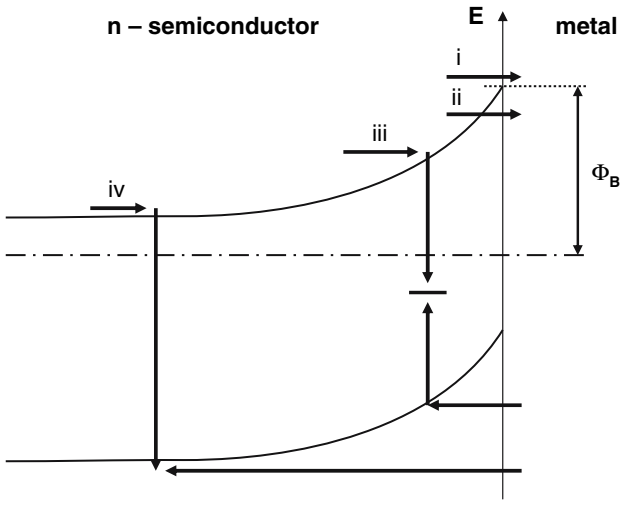


**Fig. 3** Transport processes contributing to the charge transport across a semiconductor metal/interface: (i) thermionic emission; (ii) thermionic field emission; (iii) recombination in the space charge region; and (iv) minority carrier injection

## Experimental observations

### (Cd,Zn)Te/metal contacts

Metal contacts to CdTe and ZnTe are particularly important as backside contacts for CdTe thin film solar cells. The back contact is one of the major problems of the CdTe solar cells since large barrier heights lead to non-ideal I–V characteristics [39]. The interfaces of CdTe with different metals have been systematically studied using single crystals [40–42] and polycrystalline thin films [43–46]. As an example photoemission spectra recorded during interface formation of CdTe with Au are shown in Fig. 4 [43]. An interface reaction leading to a chemical decomposition of the substrate is evident from different observations: (i) The Cd 3d

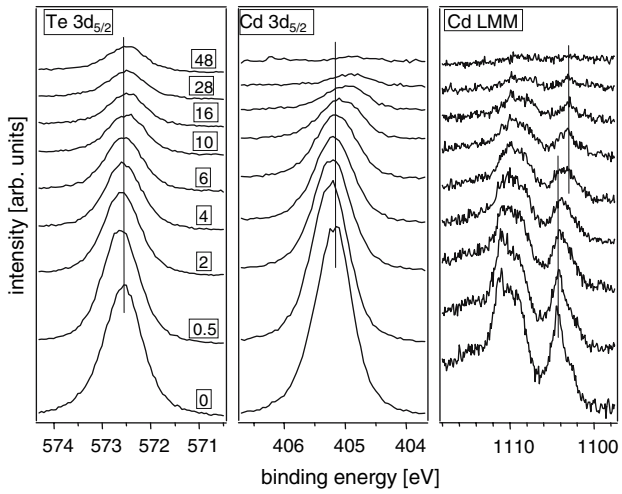


**Fig. 4** Photoelectron spectra recorded with monochromatic Al Kα radiation during deposition of Au onto a polycrystalline CdTe film. Deposition times are indicated in minutes

emission is completely attenuated with increasing Au deposition while the Te 3d intensity saturates. This indicates that Te is floating on top of the growing Au film; (ii) The Cd 3d emission shifts to lower binding energies, while the Te 3d emission shows an initial small shift to higher binding energy and then stays constant. A change of Fermi level position due to surface band bending would lead to parallel shift of both levels. The different shifts, therefore, indicates formation of new chemical species, which in the present case is metallic Cd, or Cd dissolved in the growing Au layer. This is also evident from the Cd MNN Auger emission line.

A sketch of the chemical structure of the interface of CdTe with Au as determined from the experiments is given Fig. 5. In addition, the structure of the interface between CdTe and vanadium is given for comparison. The latter shows a different type of reactivity. While the formation of Au–Te compound is not very likely, a $VTe_2$ phase is thermodynamically favourable compared to CdTe. Although different metals can react differently with CdTe, a decomposition of the CdTe layers close to the interface occurs in all cases. The released Cd might be dissolved in the growing metal layer. However, at least partially a diffusion of Cd into the CdTe substrate will also occur.

The barrier heights determined from photoemission experiments are given in Fig. 6a and are typically around 1 eV for p-type material ($\Phi_B = E_F - E_{VB}$). Interestingly, the barrier heights are very close to the energetic position of the Cd interstitial defect, which has been calculated using density functional theory [47]. Defect energy levels obtained from this calculation are reproduced in Fig. 6b. This suggests that the Fermi level position at the interface is determined by these defects, which are introduced by the chemical interface reaction. However, a charge neutrality level of CdTe has also been calculated to be at this energy [1] and might, therefore also explain the barrier heights. Additional information is therefore necessary to justify the importance of crystallographic defects for barrier formation.

More distinctive evidence for the influence of defects on contact formation is provided by studies of the interfaces of Cu and $Cu_2Te$ with CdTe (Späth B et al., unpublished results). Deposition of Cu leads to a reactive interface with formation of a $Cu_xTe$ phase and metallic Cd, associated with a barrier height of 0.95 eV. In contrast, no reaction is observed during deposition of $Cu_2Te$ onto CdTe resulting in a significantly lower barrier height. Further information is provided by the direct observation of deep defects at

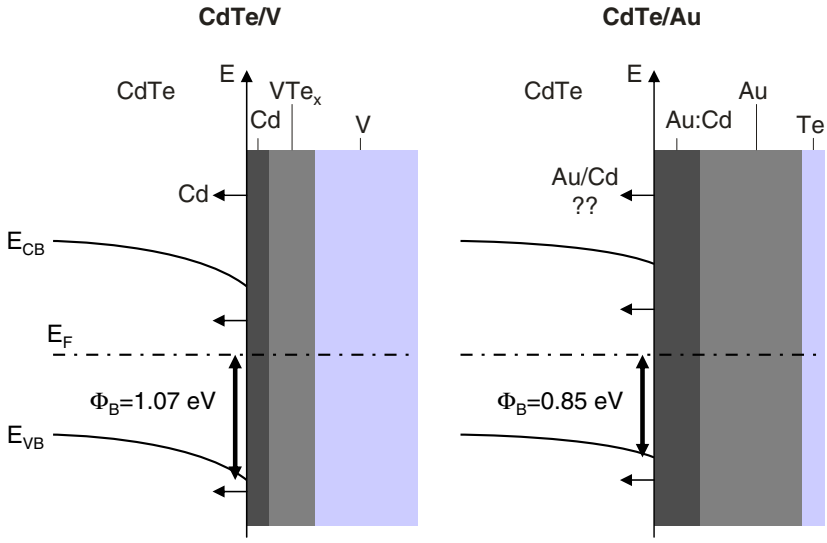


**Fig. 5** Sketch of composition of CdTe/V and CdTe/Au interfaces as derived from photoelectron spectroscopy. Both interfaces are reactive and lead to a decomposition of the CdTe surface. In the case of V deposition, the released Cd cannot be dissolved in the growing layer and V does not diffuse through the $VTe_x$ phase. The reaction is limited to a few atomic layers. Dissolution of Cd into the growing Au layer is possible and Te is floating on the Au surface

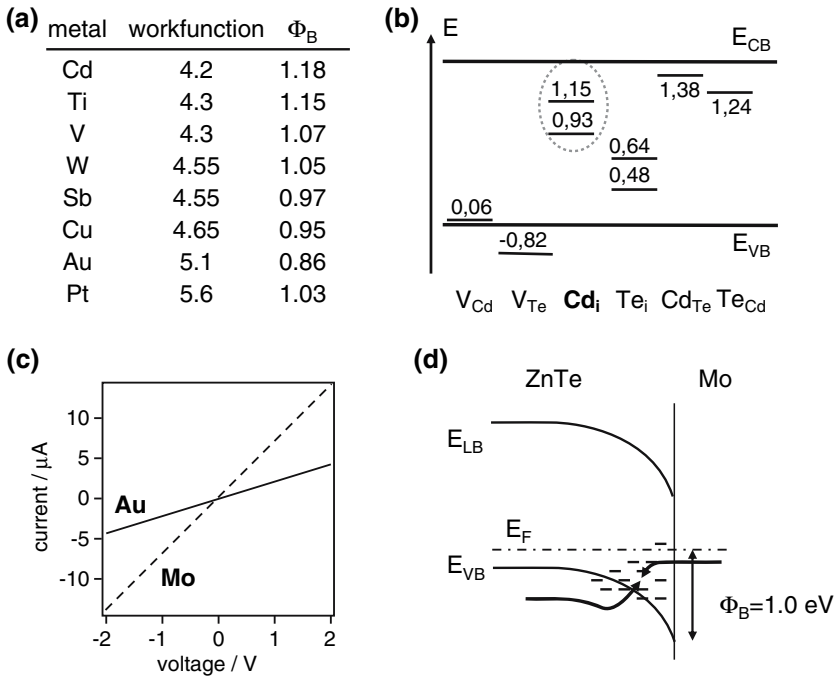


**Fig. 6** (**a**) Barrier heights for CdTe/metal interfaces as determined using photoelectron spectroscopy [43]; (**b**) Energy levels of intrinsic point defects in CdTe [47]; (**c**) Current voltage relation of ZnTe using Au and Mo metal contacts; (**d**) Anticipated current path at the ZnTe/Mo contact

CdTe/metal interfaces by cathode- and photoluminescence spectroscopy [40]. It is thus quite evident that defects contribute to contact formation for these interfaces.

Different information can be extracted from electrical measurements. Unfortunately, the conductivity of the deposited CdTe films is very poor and so electrical measurements of contact resistance are not easy. We have thus performed such measurements on doped ZnTe films. Fig. 6c shows current–voltage curves recorded from a p-type ZnTe:N layer with a carrier density of ~$10^{18}$ $cm^{-3}$ with Au and Mo contacts (2 point probe). Photoemission experiments have revealed barrier heights for Au and Mo of 0.6 and 1.0 eV, respectively [48]. Although ZnTe appears to be less reactive than CdTe, in principle the same reaction mechanisms as shown in Fig. 5 occur. The different types of reactivity again result in different barrier heights. In contrast to the large barrier heights, the current–voltage curves do not show the expected blocking behaviour of two back-to-back diodes. In addition, despite the larger barrier height, a lower contact resistance is obtained with Mo contacts. It is thus concluded, that the current transport is not over the barrier but rather through it, utilizing the defects induced by the chemical reaction at the interface as indicated schematically in Fig. 6d. The different current densities for Mo and Au contacts could then be attributed to the observed different types of interface reactions. For deposition of Mo a $MoTe_2$ phase is formed in analogy to the CdTe/V interface described above (see Fig. 5). The released Zn diffuses into the ZnTe creating a high density of defect states, while during deposition of gold most of the Zn is dissolved in the Au layer [41–43].

As discussed above, the interfacial barrier heights and transport across interfaces for the II–VI compound CdTe and ZnTe are thus closely related to the presence of defects, which are most likely introduced by contact formation. Such a behaviour is not only observed for metal contacts but also for contacts of CdTe to other materials as CdS, $VSe_2$, $In_2O_3$, $TiO_2$ and others which all lead to similar Fermi level positions at the interface (see Ref. [44] and references therein). Since it is often required to control the Fermi level position at an interface, such behaviour can cause severe limitations for device operation.

## $In_2S_3$/ZnO heterocontact

Fermi level pinning due to the presence of point defects in materials is not restricted to semiconductor/metal interfaces. In this section, we present an example for an interface between two semiconductors, which is relevant for thin film solar cells. Both materials, $In_2S_3$ and ZnO are prepared by thin film deposition under conditions where deviations from stoichiometry have to be expected.

Thin film solar cells based on polycrystalline $Cu(In,Ga)Se_2$ have shown record energy conversion

efficiencies of almost 20% [49]. The typical layer structures of these devices is Mo/Cu(In,Ga)$Se_2$/CdS/ZnO. There are a number of efforts to replace the buffer layer CdS with a less toxic material. One of the candidates studied is $In_2S_3$ [50–54]. Best cells were achieved at substrate temperatures of ~230 °C during $In_2S_3$ deposition. Experiments using CdS/$In_2S_3$ and $In_2S_3$/CdS buffer layer combinations have clearly identified that, in the presence of an $In_2S_3$/ZnO interface, the cell efficiency is significantly reduced [52, 53]. Hence, the efficiency of the cell is closely related to the properties of the $In_2S_3$/ZnO interface.

Photoelectron spectra recorded during stepwise deposition of Al-doped ZnO onto a thermally evaporated $In_2S_3$ film are shown in Fig. 7. The ZnO film is deposited by d.c. magnetron sputtering from a ceramic target, which is a process close to the one used for preparation of the cells. There is continuous decrease of the substrate emissions and also a continuous increase of the ZnO emissions. No clear evidence for an interface reaction is observed. In particular, oxidation of the substrate can be ruled out since no $SO_x$ or $InO_x$ species occur during deposition. Based on the photoemission data, the interface can be considered as atomically abrupt.

The evolution of the core-level binding energies in dependence on ZnO deposition time is shown in Fig. 8 for two interfaces with different preparation conditions of the ZnO film. The energy difference between the core-levels and the valence band maximum, which is determined for the thick films, has been subtracted from the core-level energies. The graph thus represents the position of the valence band maxima of the substrate and the overlayer in dependence on film thickness. In the experiment shown on the left the Al-doped ZnO film has been deposited using pure Ar as sputter gas. For these conditions, the Fermi level position of the thick ZnO film is determined at $E_F - E_{VB} = 3.9$ eV. Compared to the bulk band gap of $E_g = 3.3$ eV [55], this corresponds to a highly degenerate ZnO film as typically observed for such deposition conditions [56]. In contrast, ZnO films deposited with an $Ar/O_2$ sputter gas mixture (10% $O_2$) show a Fermi level for the thick film at $E_F$–$E_{VB} = 2.7$ eV.

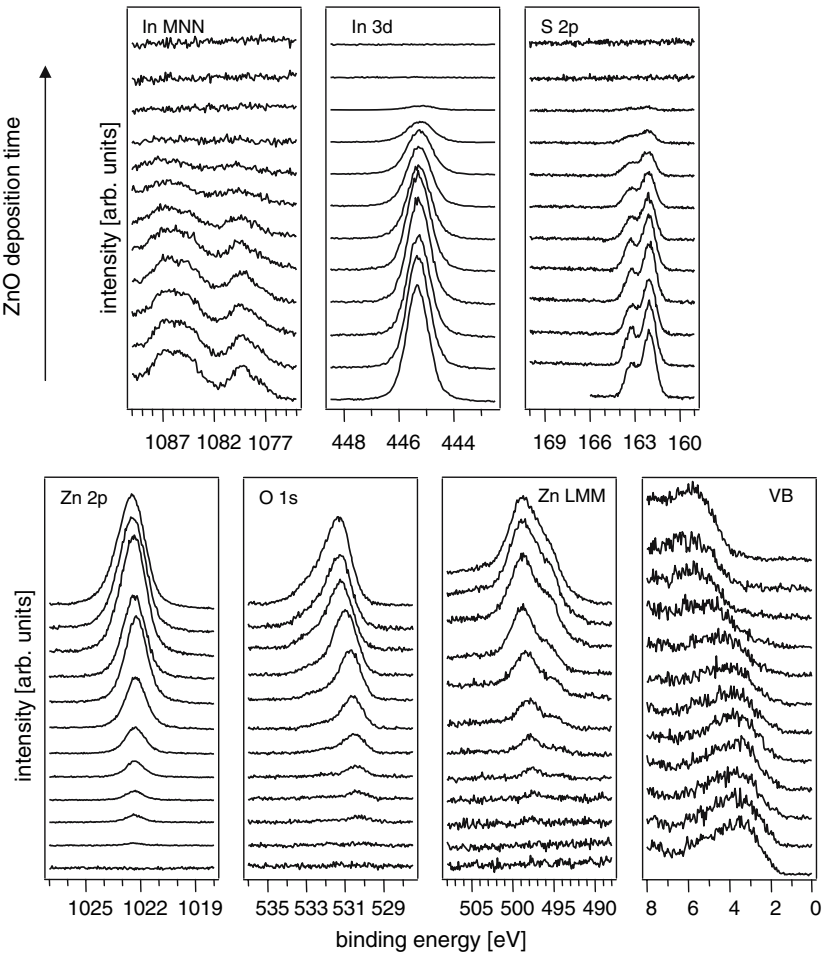


**Fig. 7** Photoelectron spectra recorded during stepwise sputter deposition of Al-doped ZnO onto evaporated $In_2S_3$. The ZnO film was deposited using pure Ar as sputter gas leading to a highly degenerate film. Monochromatic Al Kα radiation was used as excitation source

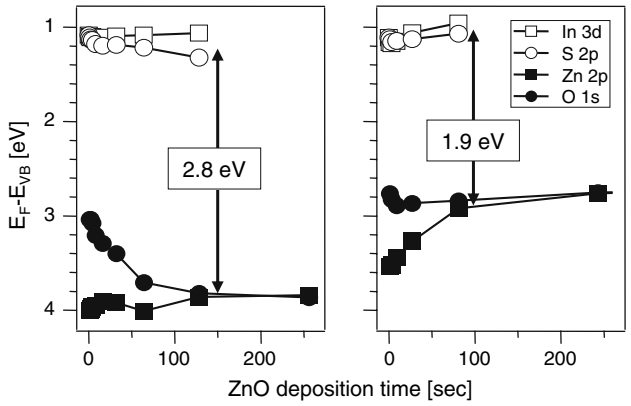


**Fig. 8** Evolution of the valence band maxima of the $In_2S_3$ substrate and the ZnO overlayer during deposition of Al-doped ZnO. The ZnO films are deposited by d.c. magnetron sputtering using pure Ar (left) and a 90% Ar/10% $O_2$ sputter gas mixture (right). The valence band maxima are derived from core-level binding energies by subtracting core-level to valence band maximum binding energy differences determined from the $In_2S_3$ substrate and the thick ZnO film, respectively

Obviously, the Al donors, which are still present in the films, are electronically compensated. Recent theoretical studies suggest that the compensation might be due to the introduction of zinc vacancies under oxygen rich conditions [57].

At low coverage the valence band maxima derived from the Zn 2p and O 1s levels do not coincide. This means that the binding energy difference between the two levels is a function of film thickness. We explain this behaviour, which is reproducibly observed for ZnO deposition [58], to an amorphous structure of the ZnO close to the interface as also found for ZnO deposition on different substrates using transmission electron microscopy [59]. The valence band offsets $\Delta E_{VB}$ for the interfaces are directly determined from the graphs in Fig. 8. It is obvious that the there is a large difference in $\Delta E_{VB}$ for the two preparation conditions. The different band offsets are related to the fact that the Fermi level does move strongly in the substrate, which is indicated by the almost constant binding energies of the In 3d and the S 2p lines.

An extended set of band alignments determined from differently prepared $In_2S_3$/ZnO interfaces are shown in Fig. 9. The $In_2S_3$ films were prepared by thermal evaporation onto substrates kept either at room temperature or at $T$ = 250 °C. For deposition at room temperature, the Fermi level at the $In_2S_3$ surface is found at 1.5±0.1 eV above the valence band maximum. This reduces to $E_F$–$E_{VB}$ ~ 1.1 eV for deposition at higher temperatures (250 °C) as for the two examples in Fig. 8.

It is evident from the results presented in Figs. 8 and 9 that the band alignment varies by as much as 1 eV. The valence band offsets at the $In_2S_3$/ZnO interfaces are to a good accuracy given by the alignment of the Fermi level positions of the films. Such behaviour is typical for metals and strongly indicates that the band alignment is controlled by a high density of defect states in the semiconductors, which pin the Fermi level in both materials. During interface formation charge is transferred from the defect states of one material to the defect states of the other and no strong band bending is thus possible to accommodate contact potential differences. The CdS/ZnO interface does not show such behaviour. For this interface, the band alignment varies only slightly with preparation conditions [60].

The different band alignments correlate well with the efficiencies of thin film solar cells with $In_2S_3$ buffers. Best conversion efficiencies are expected for a small conduction band offset, which is obtained for the situation given in Fig. 5c, where the $In_2S_3$ substrate is deposited at 250 °C and the ZnO contact film was prepared with oxygen in the sputter gas, which results in an un-doped film. The conditions used in this experiment are the same as those for which best conversion efficiencies of the solar cells are obtained [51, 54].

## $CuInSe_2$/CdS heterocontact

Interface formation of the semiconductor Cu(In,-Ga)$Se_2$ indicates that Cu diffuses from the surface into the material when the Fermi level moves upwards in the band gap by contact formation [34, 61–63]. The effect is observed for surfaces of single crystals, which exhibit a stoichiometric composition and have a Fermi level close to the valence band. In contrast, surfaces of thin film Cu(In,Ga)$Se_2$ often show segregation of a Cu-deficient $Cu(In,Ga)_3Se_5$ phase and have a Fermi level close the conduction band [34, 64, 65]. For such surfaces, a Cu enrichment during interface formation, associated with a downward shift of the Fermi level, has been observed. The different behaviour of Cu-rich and Cu-poor thin film samples is illustrated in Fig. 10. The preparation of clean Cu-poor Cu(In,Ga)$Se_2$ surfaces follows the de-capping procedure, which is described in detail elsewhere [34, 65]. Cu rich surfaces are prepared by KCN etching of films deposited with slight Cu excess. The etching procedure has been carried out in nitrogen flow in a chamber, which is directly connected to the spectrometer system. It is evident that Cu(In,Ga)$Se_2$ exhibits large changes of composition during interface formation, which is

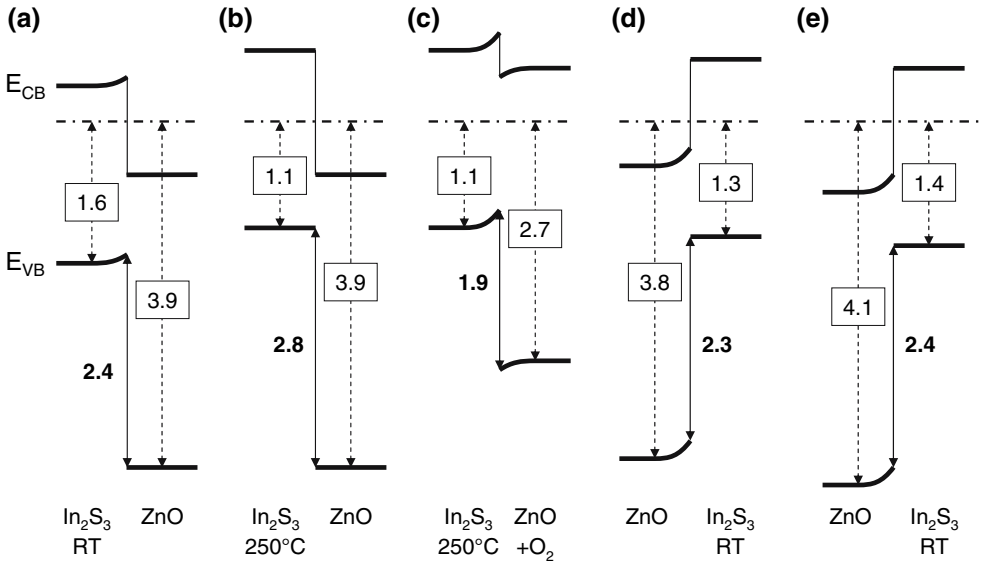


**Fig. 9** Band alignment of differently prepared ZnO/$In_2S_3$ interfaces. Substrates are given to the left and overlayers to the right of each interface. ZnO films were doped with 2 wt% Al and are deposited using magnetron sputtering at room temperature. Except for experiment (**c**), where 10% of oxygen was added to the sputter gas, all ZnO films were deposited with pure Ar. $In_2S_3$ films were prepared by thermal evaporation at different substrate temperatures. Band gaps used to draw the conduction band positions are 3.3 eV for ZnO and 1.9 eV for $In_2S_3$

related to a high mobility of Cu and to changes in the electric surface potentials.

The interface between $CuInSe_2$ and CdS provides a nice example for a self-compensation mechanism occurring at an interface. The self-compensation mechanism is also illustrated in Fig. 10. The explanation requires understanding the Fermi energy dependence of defect formation energies [66]. Defect formation energies of negatively charge defects (acceptors with a Fermi energy above the defect energy) decrease with increasing Fermi energy, while the formation energy of positively charges defects (donors with the Fermi energy below the defect energy) increase with increasing Fermi energy. Starting now from a p-doped substrate surface the Fermi level at the surface can be raised due to adsorption of the contact material. When the Fermi energy reaches the defect energy level of the interstitial Cu donor, its charge state changes from negative to neutral. Its defect formation enthalpy thus no longer increases with a rising $E_F$, while those of

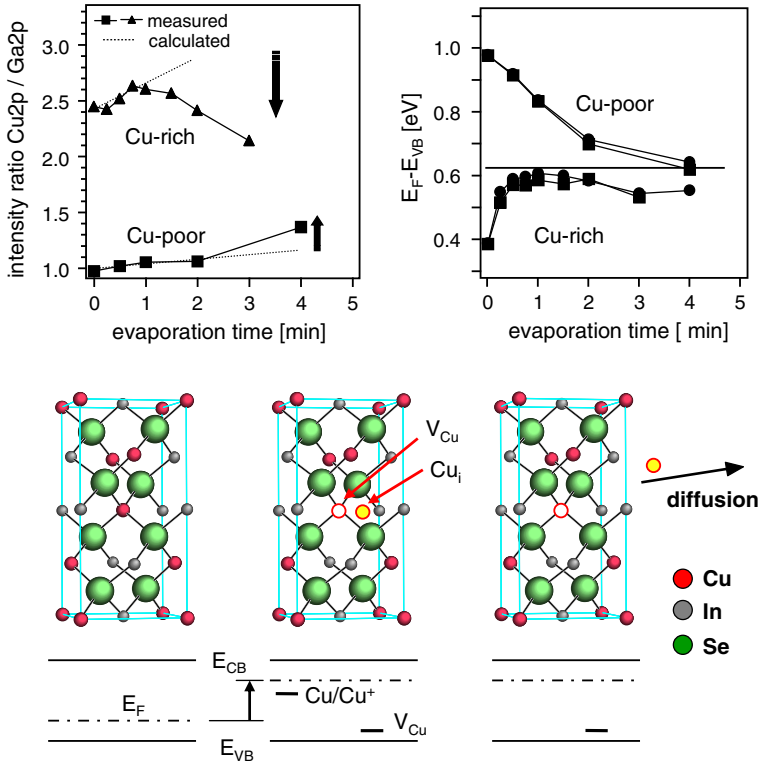


**Fig. 10** (Top) Evolution of Cu/Ga intensity ratio and Fermi level position for a polycrystalline $Cu(In,Ga)Se_2$ substrate in dependence on CdS deposition time determined using photoelectron spectroscopy. The straight lines indicate the increase the intensity ratio, which is expected because of the different information depths of the Cu 2p and the Ga 2p lines. (Bottom) Sketch of Cu depletion induced by an upward shift of the Fermi level due to contact formation (self-compensation mechanism)

the Cu vacancy acceptor level $V_{Cu}$ is further decreasing. Raising $E_F$ above the defect energy of $Cu_i$ will thus lead to a net decrease of the formation of the Frenkel defect pair ($Cu_i$, $V_{Cu}$). As interstitial Cu can easily diffuse in $CuInSe_2$ [67], it will be depleted near the surface resulting in an increase of the acceptor concentration and thereby limit further movement of the Fermi energy.

## Conclusions

Today the influence of non-stoichiometry on the interface formation is not well studied. Nevertheless there is steadily increasing evidence from different fields that deviations from stoichiometry are essential in establishing most important interface properties as band alignment (barrier heights) and transport properties. In many cases the picture of abrupt interfaces with a well defined band alignment being unique for a given material combination and simple transport processes neglecting defect states in the band gap is not appropriate. However, the microscopic origin of the point defects at interfaces, their individual contribution to band alignment, current transport and electronic device properties is yet mostly unclear and needs to be resolved for different cases.

## References


1. Mönch W (2003) Electronic properties of semiconductor interfaces. Springer-Verlag, Heidelberg
2. Van De Krol R, Tuller HL (2002) Solid State Ionics 150:167
3. Sze SM (1981) Physics of semiconductor devices. John Wiley & Sons, New York
4. Fonash SJ (1981) Solar cell device physics. Academic Press, New York
5. Kao KC, Hwang W (1981) Electrical transport in solids. Pergamon Press, Oxford
6. Franciosi A, Van De Walle CG (1996) Surf Sci Rep 25:1
7. Peressi M, Binggeli N, Baldereschi A (1998) J Phys D 31:1273
8. Yu ET, McCaldin JO, McGill TC (1992) Solid State Phys 46:1
9. Tung RT (1993) J Vac Sci Technol B 11:1546
10. Kroemer H (1993) J Vac Sci Technol B 11:1354
11. Capasso F, Margaritondo G (1987) Heterojunction band discontinuities. North-Holland, Amsterdam
12. Kurtin S, McGill TC, Mead CA (1969) Phys Rev Lett 22:1433
13. Cowley AM, Sze SM (1965) J Appl Phys 36:3212
14. Tersoff J (1984) Phys Rev B 30:4874
15. Cardona M, Christensen NE (1987) Phys Rev B 35:6182
16. Heine V (1965) Phys Rev 138:1689
17. Louie SG, Chelikowsky JR, Cohen ML (1977) Phys Rev B 15:2154
18. Harrison WA, Klepeis E (1988) Phys Rev B 37:864
19. Spicer WE, Chye PW, Skeath PR, Su CY, Lindau I (1979) J Vac Sci Technol 16:1422
20. Spicer WE, Lilienthal-Weber Z, Weber E, Newman N, Kendelewicz T, Cao R, McCants C, Mahowald R, Miyano K, Lindau I (1988) J Vac Sci Technol B 6:1245
21. Walukiewicz W (1987) J Vac Sci Technol B 5:1062
22. Walukiewicz W (1998) Phys Rev B 37:4760
23. Zhang SB, Wei S-H, Zunger A (1998) J Appl Phys 83:3192
24. Zhang SB, Northrup JE (1991) Phys Rev Lett 67:2339
25. Kröger FA (1964) The chemistry of imperfect crystals. North-Holland, Amsterdam
26. Smyth DM (2000) The defect chemistry of metal oxides. Oxford University Press, Oxford
27. Maier J (2004) Physical chemistry of ionic materials. Wiley-VCH, Weinheim
28. Zur A, McGill TC, Smith DL (1983) Phys Rev B 28:2060
29. Inoue A, Izumisawa K, Uwe H (2001) Jpn J Appl Phys 40:353
30. Shimizu T, Okushi H (1999) J Appl Phys 85:7244
31. Takatani S, Miki H, Kushida-Abdelghafar K, Torii K (1999) J Appl Phys 85:7784
32. Baniecki JD, Laibowitz RB, Shaw TM, Saenger KL, Duncombe PR, Cabral C, Kotecki DE, Shen H, Liand J, Mae QY (1999) J Eur Ceram Soc 19:1457
33. Rubini S, Milocco E, Sorba L, Pelucchi E, Franciosi A, Garulli A, Parisini A, Zhuang A, Bauer G (2001) Phys Rev B 63:155312
34. Klein A, Schulmeyer T (2006) In: Siebentritt S, Rau U (eds) Wide gap chalcopyrites. Springer Verlag, Heidelberg
35. Säuberlich F, Klein A (2003) Mater Res Soc Symp Proc 763:B9.10
36. Briggs D, Seah MP (1983) Practical surface analysis by Auger and X-Ray photoelectron spectroscopy. John Wiley & Sons, New York
37. Klein A, Pettenkofer C, Jaegermann W, Lux-Steiner MC, Bucher E (1994) Surf Sci 321:19
38. Rhoderick EH, Williams RH (1988) Metal-semiconductor contacts. Clarendon Press, Oxford
39. Nollet P, Burgelman M, Degrave S (2000) Thin Solid Films 361(362):293
40. Shaw JL, Viturro RE, Brillson LJ, Kilday D, Kelly MK, Margaritondo G (1988) J Vac Sci Technol A 6:2752
41. Friedman DJ, Lindau I, Spicer WE (1988) Phys Rev B 37:731
42. Trafas BM, Meyer III HM, Aldao CM, Siefert RL, Vos M, Xu F (1990) J Vac Sci Technol A 8:2055
43. Kraft D (2004) Präparation und charakterisierung von dünnschichtmaterialsystemen für die rückkontaktbildung bei polykristallinen CdTe-dünnschichtsolarzellen. Thesis, Technische Universität Darmstadt
44. Jaegermann W, Klein A, Fritsche J, Kraft D, Späth B (2005) Mater Res Soc Symp Proc 865:F6.1
45. Klein A (2004) Adv Sol State Phys 44:13
46. Dharmadasa IM (1998) Prog Crystal Growth Charact 36:249
47. Wei S-H, Zhang SB (2002) Phys Rev B 66:155211
48. Späth B, Fritsche J, Klein A, Jaegermann W (2005) Mater Res Soc Symp Proc 865:F8.3
49. Ramanathan K, Contreras MA, Perkins CL, Asher S, Hasoon FS, Keane J, Young D, Romero M, Metzger W, Noufi R, Ward J, Duda A (2003) Prog Photovolt Res Appl 11:225
50. Hariskos D, Spiering S, Powalla M (2005) Thin Solid Films 480–481:99
51. Spiering S, Eicke A, Hariskos D, Powalla M, Naghavi N, Lincot D (2004) Thin Solid Films 451(452):562

52. Nguyen Q, Rau U, Mamor M, Orgassa K, Schock HW, Werner JH (2001) Proceedings of the 17th European photovoltaic solar energy conference, München
53. Nguyen Q, Orgassa K, Kötschau I, Rau U, Schock HW (2003) Thin Solid Films 431(432):330
54. Strohm A, Eisenmann L, Gebhardt RK, Harding A, Schlötzer T, Abou-Ras D, Schock HW (2005) Thin Solid Films 480(481):162
55. Madelung O (1996) Semiconductors basic data, 2nd edn. Springer Verlag, Berlin
56. Ellmer K (2000) J Phys D 33:R17
57. Erhart P, Klein A, Albe K (2005) Phys Rev B 72:085213
58. Venkata Rao G, Säuberlich F, Klein A (2005) Appl Phys Lett 87:032101
59. Yoshino Y, Inoue K, Takeuchi M, Ohwada K (1998) Vacuum 51:601
60. Säuberlich F, Fritsche J, Hunger R, Klein A (2003) Thin Solid Films 431(432):378
61. Klein A, Jaegermann W (1999) Appl Phys Lett 74:2283
62. Klein A, Fritsche J, Jaegermann W, Schön JH, Kloc C, Bucher E (2000) Appl Surf Sci 166:508
63. Klein A, Löher T, Pettenkofer C, Jaegermann W (1996) J Appl Phys 80:5039
64. Schmid D, Ruckh M, Schock HW (1996) Appl Surf Sci 103:409
65. Schulmeyer T, Hunger R, Lebedev M, Jaegermann W, Klein A, Kniese R, Powalla M (2005) Thin Solid Films 480(481):110
66. Zunger A (2003) Appl Phys Lett 83:57
67. Lyubomirsky I, Rabinal MK, Cahen D (1997) J Appl Phys 81:6684